Title

Direct Measurements of Colloidal Solvophoresis under Imposed Solvent and Solute Gradients

Journal

Langmuir, 31(15)

ISSN

0743-7463

Authors

Paustian, Joel S

Angulo, Craig D

Nery-Azevedo, Rodrigo

et al.

Publication Date

2015-04-21

DOI

10.1021/acs.langmuir.5b00300

Peer reviewed

Langmuir

Article

pubs.acs.org/Langmuir

Direct Measurements of Colloidal Solvophoresis under Imposed Solvent and Solute Gradients

Joel S. Paustian,[†] Craig D. Angulo,[†] Rodrigo Nery-Azevedo,[†] Nan Shi,[†] Amr I. Abdel-Fattah,[‡] and Todd M. Squires*[,†]

[†]Department of Chemical Engineering, University of California, Santa Barbara, Santa Barbara, California 93106, United States

[‡]Saudi Aramco, Dhahran, Saudi Arabia

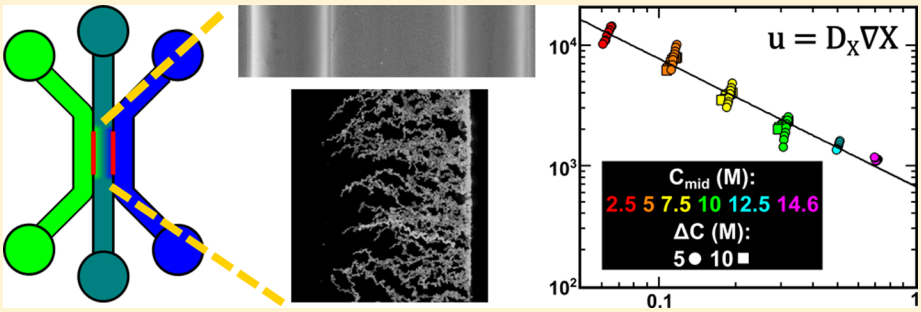

ABSTRACT: We describe a microfluidic system that enables direct visualization and measurement of diffusiophoretic migration of colloids in response to imposed solution gradients. Such measurements have proven difficult or impossible in macroscopic systems due to difficulties in establishing solution gradients that are sufficiently strong yet hydrodynamically stable. We validate the system with measurements of the concentration-dependent diffusiophoretic mobility of polystyrene colloids in NaCl gradients, confirming that diffusiophoretic migration velocities are proportional to gradients in the logarithm of electrolyte concentration. We then perform the first direct measurement of the concentration-dependent "solvophoretic" mobility of colloids in ethanol−water gradients, whose dependence on concentration and gradient strength was not known either theoretically or experimentally, but which our measurements reveal to be proportional to the gradient in the logarithm of ethanol mole fraction. Finally, we examine solvophoretic migration under a variety of qualitatively distinct chemical gradients, including solvents that are miscible or have finite solubility with water, an electrolyte for which diffusiophoresis proceeds *down* concentration gradients (unlike for most electrolytes), and a nonelectrolyte (sugar). Our technique enables the direct characterization of diffusiophoretic mobilities of various colloids under various solvent and solute gradients, analogous to the electrophoretic ζ-potential measurements that are routinely used to characterize suspensions. We anticipate that such measurements will provide the feedback required to test and develop theories for solvophoretic and diffusiophoretic migration and ultimately to the conceptual design and engineering of particles that respond in a desired way to their chemical environments.

INTRODUCTION

Colloids and polymers migrate in response to concentration gradients via diffusiophoresis,[1−4] which provides an important (but often overlooked) mechanism for micro- and nanoparticle transport within multicomponent solutions. In particular, surfaces that react, dissolve, or equilibrate naturally establish concentration gradients of various species and can enhance or retard the deposition of particles or polymers. In some cases, this deposition is intentional—for example, in the growth of polymer films and other coatings[1,5,6]—whereas in other cases it is undesired (e.g., contamination and fouling[7]). Diffusiophoresis has also received recent attention for its importance to self-propelling particles[8−11] and active matter[12−14] as well as direct observations of exclusion zones around membranes[15] and diffusioosmotic "pumps" established by dissolving salt crystals.[16] In subsurface applications like oil recovery and environmental remediation, diffusiophoresis can play roles that are beneficial (e.g., enhancing surface wettability alteration, contaminant immobilization or hydrocarbon recovery) or detrimental (e.g., promoting the deposition and bridging of fine particles and therefore trigger pore clogging and formation damage).

Direct characterization of diffusiophoresis will be essential to predict, understand, and engineer the response of colloids in varying environments. Nonetheless, direct observation and measurement of diffusiophoresis has remained extremely challenging, since macroscopically imposed solution gradients that are strong enough to drive measurable diffusiophoresis often introduce density gradients that drive hydrodynamic instabilities. Unlike electrophoresis, for which commercial

Received: January 25, 2015
Revised: March 28, 2015

DOI: 10.1021/acs.langmuir.5b00300
Langmuir XXXX, XXX, XXX−XXX

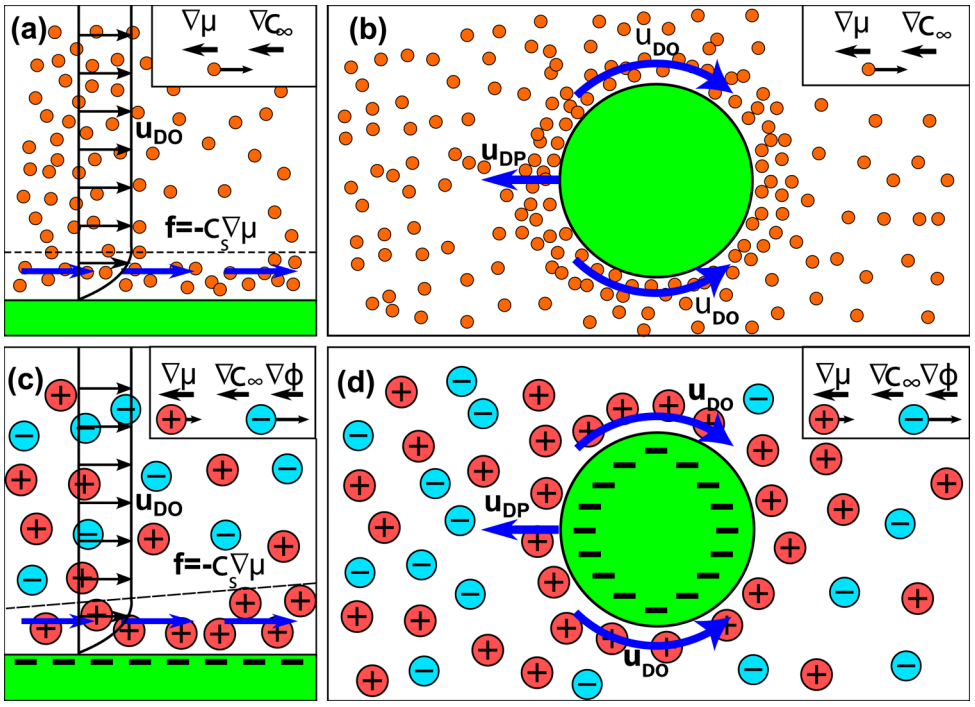

Figure 1. (a) Diffusioosmotic flow occurs along a surface adjacent to a bulk concentration gradient ∇c_∞ (and corresponding chemical potential gradient $\nabla\mu$). A solute has excess concentration $c_s = c - c_\infty$ along the surface. A net body force $-c_s\nabla\mu$ on the excess layer drives a diffusioosmotic slip flow u_{DO} along the surface. (b) Diffusioosmotic slip along a colloidal particle results in diffusiophoresis. (c) The diffusioosmotic velocity u_{DO} of a charged particle in an electrolyte gradients generally has both electroosmotic and chemiosmotic contributions. The chemiphoretic slip is driven by concentration gradients within the double layer along the surface, giving a chemiosmotic slip that is directed *down* electrolyte gradients. The electroosmotic component results from asymmetric ion diffusivities and can be directed either up or down the electrolyte gradient. If the anion has higher diffusivity than the cation, then its tendency to "outrun" the cation establishes an electric field in solution, directed down the electrolyte concentration gradient (inset). This electric field drives particles into electrophoretic migration either up or down the electrolyte gradient, depending on the charge of the particle and relative ion diffusivities. (d) Diffusioosmotic slip along the surface of a colloid in an electrolyte gradient is gives rise to diffusiphoretic migration either up or down the gradient, depending on the sign of the electrophoretic contribution, and the relative magnitudes of the chemiphoretic and electrophoretic contributions.

instruments are routinely used to measure the electrokinetic ζ-potential, no such capability exists for diffusiophoresis. Instead, diffusiophoretic mobilities have been extracted by measuring particle deposition onto membranes[2,17] and transient migration in stopped-flow fluidic devices.[18]

Recent advances in microfluidics, however, have enabled the direct visualization of diffusiophoretic migration, since the small dimensions of microfluidic devices are effective in suppressing buoyancy-driven instabilities.[19] Colloidal streams have been focused and spread using coflowing streams of varying salinity,[20,21] and agarose-based microfluidic devices have been used to drive the diffusiophoretic motion of colloids and DNA under imposed salinity gradients.[22,23] However, these methods have not yet been used to directly measure concentration-dependent diffusiophoretic mobilities, nor to measure the diffusiophoretic migration under nonelectrolyte gradients, which had been predicted theoretically[4,24,25] and verified experimentally.[18] Moreover, only one published report describes colloidal migration under solvent gradients (solvophoresis),[26] based on macroscopic measurements that tracked the turbidity in the vicinity of horizontal interfaces between miscible solutions as it developed over several days.[26]

We have recently developed a method to impose local solute and solvent gradients within microchannels, which enabled the first direct microscopic visualization of solvophoretic migration.[27] To set up strong gradients within channels, we photopolymerize thin hydrogel membranes into so-called "microfluidic stickers" devices[28] made from the UV-curable optical adhesive NOA-81 (Norland), based on their superior solvent-compatibility compared with standard PDMS devices. Our method allows high-resolution velocity measurements of diffusiophoresis under diverse chemical gradients. In this work, we use this experimental system to perform quantitative measurements of the diffusiophoretic and solvophoretic mobilities of particles in both salinity and ethanol–water gradients. In particular, our system enables us to impose both the local concentration as well as the strength of the gradient and therefore to measure these phoretic mobilities under a variety of conditions. Our experiments in ethanol–water gradients, for example, reveal a previously unknown relation $u_{SP} = D_{SP}\nabla \ln X$ between the average solvophoretic velocity u_{SP} and the ethanol mole fraction X by the mobility D_{SP}.

Diffusiophoresis is the phoretic analogue of diffusioosmotic flow, which is driven along a stationary surface by a bulk concentration gradient. A solute with bulk concentration c_∞ and constant gradient ∇c_∞ gives rise to a bulk chemical potential gradient $\nabla\mu_\infty = k_B T\nabla \ln(c_\infty/c^*)$ (Figure 1a). Solute–surface interactions, such as van der Waals forces, excluded volume forces, or hydration forces, establish an excess solute concentration $c_s(x,y)$ in a thin "excess layer" that differs from that in the bulk via some excess $c_s = c - c_\infty$. The concentration gradient puts an entropic force on the excess layer, resulting in body force $f = -c_s\nabla\mu$ on the fluid within the excess layer, and drives a diffusioosmotic slip flow.

DOI: 10.1021/acs.langmuir.5b00300
Langmuir XXXX, XXX, XXX–XXX

Diffusiophoretic migration is driven by the diffusioosmotic flow along the surface of a freely floating colloidal particle (Figure 1b). The diffusiophoretic velocity under dilute, nonelectrolyte gradients, assuming zero Peclet number, was derived by Anderson and Prieve[24]

$$u_{DP} = \frac{k_B T}{\eta} L^2 \nabla c \int_0^\infty y \left(\exp \frac{-\phi(y)}{k_B T} - 1 \right) dy \quad (1)$$

with Boltzmann's constant k_B, temperature T, viscosity η, concentration c, solute−surface interaction energy ϕ, characteristic length scale L for the excess layer, and (scaled) distance from the surface y/L. The integral gives the first moment of the excess solute distribution.

The most extensive studies have occurred for diffusioosmosis and diffusiophoresis within electrolyte gradients, for which two mechanisms arise. First, anions and cations with different diffusivities naturally establish electric fields as their gradients relax diffusively, which drive electroosmosis and electrophoresis along charged surfaces (Figure 1c,d). Second, the osmotic pressure difference along the colloid surface also causes a "chemiphoretic" contribution to the diffusiophoretic velocity. The diffusiophoretic velocity in a binary electrolyte is given by the sum of these contributions[4,29]

$$u_{DP} = \frac{\varepsilon}{\eta} \frac{k_B T}{ze} \left(\zeta\beta + \frac{4 k_B T}{ze} \ln \cosh \frac{ze\zeta}{4 k_B T} \right) \nabla \ln \left(\frac{c}{c^*} \right) \quad (2)$$

where the parameter β reflects differences in ion mobility

$$\beta = \frac{D_+ - D_-}{D_+ + D_-} \quad (3)$$

with ion diffusivities $D_\pm$ and with permittivity ε, zeta-potential ζ, ion concentration c, and (arbitrary) reference concentration c^*, assuming zero Peclet number and symmetric z:z electrolyte.

The first term in eq 2 is the electrophoretic contribution which can be directed either up or down the gradient, and the second term reflects the chemiphoretic contribution, which is always directed up the gradient. Colloidal diffusiophoresis typically proceeds up electrolyte gradients but can in certain circumstances migrate down gradients[29] (e.g., Figure 7d).

Magnitudes for diffusiophoretic velocities may be more easily estimated by scaling the ζ-potential with the thermal potential

$$\tilde{\zeta} = \frac{ze\zeta}{k_B T} \quad (4)$$

whereupon eq 2 can be expressed as

$$u_{DP} = \frac{3}{2z^2} D_B \left(\tilde{\zeta}\beta + 4 \ln \cosh \frac{\tilde{\zeta}}{4} \right) \nabla \ln \left(\frac{c}{c^*} \right) \quad (5)$$

where

$$D_B = \frac{k_B T}{6\pi\eta\lambda_B} \quad (6)$$

is the diffusivity of a sphere whose radius is given by the Bjerrum length

$$\lambda_B = \frac{e^2}{4\pi\varepsilon k_B T} \quad (7)$$

The Bjerrum length is approximately $\lambda_B \sim 0.7$ nm in water at room temperature, so that $D_B \sim 350\ \mu m^2/s$. Expressions for the diffusiophoretic mobility in multicomponent electrolyte gradients are also available.[30]

The goals of this work are (1) to propose and validate a new experimental system for diffusiophoresis measurements under diverse chemical gradients and (2) apply the experimental system to study solvophoresis. We start with a discussion of the device fabrication, experimental setup, and data analysis method. Next, the diffusiophoretic velocity is measured in NaCl gradients, where we expect to see the $u_{DP} \sim \nabla \ln(c/c^*)$ scaling described in eq 2 and observed in recent microfluidics experiments in agarose channels.[22,23] This is followed with solvophoretic mobility measurements in ethanol−water gradients and experiments showing diffusiophoresis and solvophoresis in diverse chemical gradients. We conclude by discussing the implications of our results and future directions for this new experimental platform.

METHODS

Device Fabrication. A three-channel device was used to impose concentration gradients across colloidal solutions (Figure 2a). The channels were fabricated in microfluidic stickers devices[28] as described previously. To aid in hydrogel membrane fabrication, the channel hydraulic resistances were matched[31] which prevented PEG-DA solution from building up in unequal amounts in the device inlets, causing stray hydrostatic flows during cross-linking. The dimensions of each of the three channels were 1 cm long × 150 μm wide × 10 μm deep.

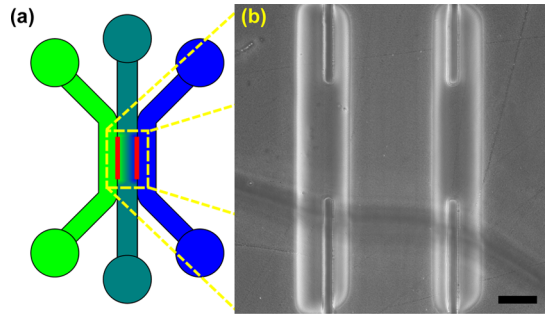

Figure 2. (a) Solution gradients across a central sample channel are established using a three-channel microfluidic device, wherein distinct reservoir solutions ("green" and "blue") were maintained adjacent to hydrogel dialysis membranes via constant flow in the left and right "reservoir" channels. (b) Close-up of sample analysis region, showing gels that have been photopolymerized into well-defined gaps in the (impermeable) walls between reservoir and sample channels. The PEG-DA hydrogel membranes provide strong resistance to transmembrane flow yet enable the diffusive transport of solute and solvent between the reservoir and sample channels, allowing a steady gradient to be imposed. Phase contrast, scale bar: 50 μm.

Hydrogels were prepared using the "hydrogel membrane microwindow (HMM)" procedure described previously.[27] This method allows strong gradients to be established perpendicular to and entirely within the imaging plane, and the small channel dimensions suppress the hydrodynamic flows and instabilities often associated with strong concentration gradients. Although the transmembrane flow velocities arising with HMMs prepared in that work were already quite small small ($u_P \lesssim 1\ \mu$m/s), the diffusiophoretic migration measured in the present work ($u_{DP} \sim 1\ \mu$m/s) can be slow enough that even smaller transmembrane flows are required. We reduce such transmembrane flows by increasing the thickness of each hydrogel membrane to ∼100 μm.

Freshly prepared PEG_M-diacrylate (PEG-DA, M = 400 g/mol, Polysciences Inc.) were mixed using 95% v/v PEG-DA and 5% v/v photoinitiator (2-hydroxy-2-methylpropiophenone, Sigma-Aldrich).

DOI: 10.1021/acs.langmuir.5b00300
Langmuir XXXX, XXX, XXX−XXX

The UV lamp was set to 30 mW/cm^2 (measured at an empty objective slot). The 500 μm wide photomask slits were inserted into the microscope and aligned as described previously. The PEG-DA solution was injected until NOA-81 channels were filled, then the syringe was disconnected, and 2 min was allowed for flows to relax. A 40 ms exposure was then used for each hydrogel. Finally, the channels were rinsed with DI water for at least 5 min. The procedure resulted in hydrogels that were 70−100 μm wide (Figure 2b). No trans-HMM flows were observed, which was verified by placing DI water in all channels (with colloids in the center channel), setting all inlets to the standard operational pressure (described below), and recording colloid motion in the center channel over several minutes.

Experimental Method. Figure 3 summarizes the experimental setup. Experiments were performed using an inverted microscope

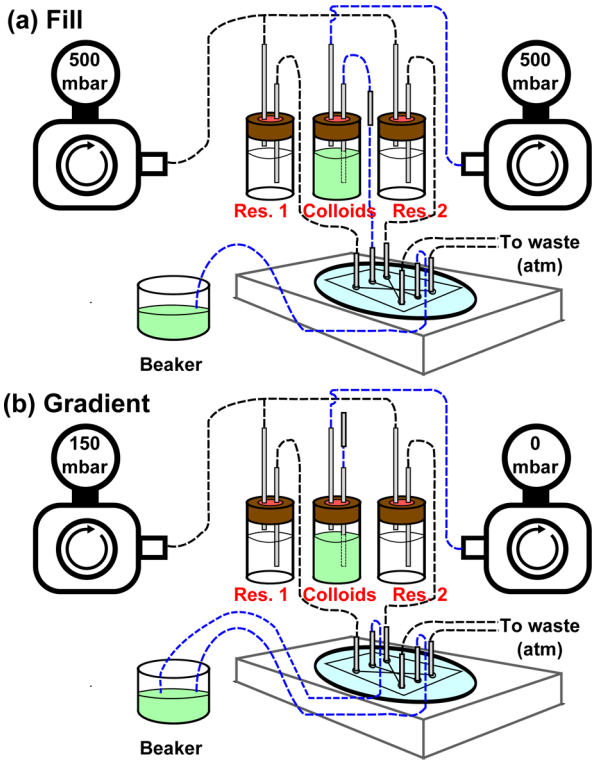

Figure 3. (a) Channels are filled by pressurizing sealed vials connected to each of the three channels. Outflows from reservoir channels are discarded, while the sample channel flows into an external beaker. Flow is maintained in the outer channels, setting up a gradient across the center channel that drives diffusiophoresis. (b) Flow in the center channel is quickly stopped by submerging the inlet tubing into the beaker along with the outlet tubing, then disconnected from the source vial tubing. This ensures no free fluid surface exists at either end of the tubing, thereby preventing capillary pressure gradients that would otherwise drive flows along the sample channel.

(Nikon TE2000U). The main experimental challenge is to rapidly stop flow in the center channel (in order to initialize the gradient). To accomplish this, the inlet and outlet tubing must be brought to exactly the same hydrostatic pressure without introducing bubbles into the tubing.[32] Bubbles also must be fully eliminated from the center channel to avoid flows driven by capillary pressure.

Solutions were prepared and placed in vials with septa. The center solution contained 0.1 wt % 1 μm diameter fluorescent particles (Bangs Laboratories FS03F). To control the pressure of the vials, tubing was connected from precision air pressure regulators with digital pressure gauges. The septum was punctured with syringe needles, which were connected with Luer Lock connections to Tygon microbore tubing (0.02 in. i.d. × 0.06 in. o.d., Cole-Parmer). The center channel inlet tubing had a metal pin inserted in the middle, where the tubing could be easily removed.

Initially, channels were filled by pressurizing each inlet to 500 mbar (Figure 3a). After filling the middle channel, it was carefully checked for bubbles, which tend to stick at the low-pressure outlet of the microchannel. If bubbles were present, the pressure at the middle channel inlet was increased to 1 bar and the outlet tubing was pinched shut with a tweezers to bring the entire channel to high pressure. The tubing was held shut until the bubbles dissolved, which could take several minutes.

After the outlet tubing had been filled, it was placed into a beaker reservoir containing the same buffer solution as the center channel. Then, the metal pin in the inlet tube was submerged in the beaker reservoir. The pressure supply to the center channel was decreased to 20 mbar, and the pressure supply to the outer channels was decreased to 150 mbar. The focus was adjusted to the center of the channel using a 20× ELWD objective (NA = 0.45). The video recording was started (Andor iXon 885 fluorescence camera), and the metal pin was removed from the inlet tubing while submerged underwater (Figure 3b) to rapidly stop the flow. The pressure to the center channel vial was turned off to prevent leakage, and the tubing was raised above the vial to allow drainage. Flow velocity along the center channel could typically be reduced to 0.1−2 μm/s using this method.

In each experiment, videos were recorded with 0.1 s exposure times for 100 s. Figure 4a shows a superposed image of the motion of colloidal particles under an ethanol−water gradient.

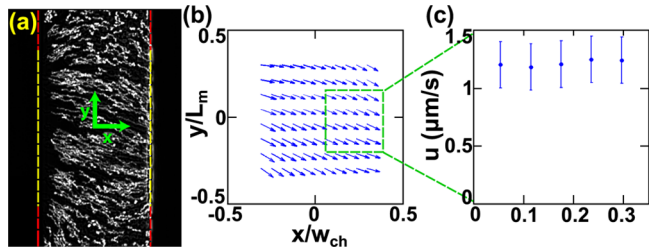

Figure 4. (a) Epifluorescence video microscopy is used to record solvo/diffusiophoretic migration of particles. (b) Particle velocity fields are obtained from experimental videos using μPIV, focusing on the region where the solution gradient is imposed. Further analysis is performed using a smaller region (green box) that is selected to better capture regions with nearly unidirectional gradients and to ensure sufficient particle concentrations throught the video. In particular, velocities are analyzed only on the side of the channel toward which particles migrate. Only the central third ($L_m/6 < y < L_m/6$) of the gradient region is analyzed to reduce two-dimensional "fringing" fields near membrane edges and to capture a more closely one-dimensional gradient. (c) The velocity field within the green box is averaged across the y-direction and plotted along the gradient.

Data Analysis. *Velocity Measurement.* Microparticle image velocimetry (μ-PIV) was used to measure the velocity profile from the recorded image sequences (Figure 4b), with 10 μm depth of correlation.[33,34] The movies contained a brief transient immediately after flow stoppage. To obtain the steady state velocity, PIV was performed only on the frames at least 5 s after flow stoppage. The initial frame was chosen by this method. The final frame was set when beads became depleted across half the channel width. The analysis was performed on the channel half where beads were steadily present ($x >$ 0 in Figure 4). A steady profile was confirmed by plotting the profile for various earlier and later increments. The channel was broken into 64 × 128 pixel interrogation regions with 75% overlap. An average image was subtracted from each image before performing the correlation. The resulting velocity field was averaged over the middle four points in y (corresponding to the central third of the gradient region), giving an average profile in x (Figure 4c).

Gradient Calculation. The concentration gradient depends upon the channel geometry and solute diffusivities. An imposed concen-

DOI: 10.1021/acs.langmuir.5b00300
Langmuir XXXX, XXX, XXX−XXX

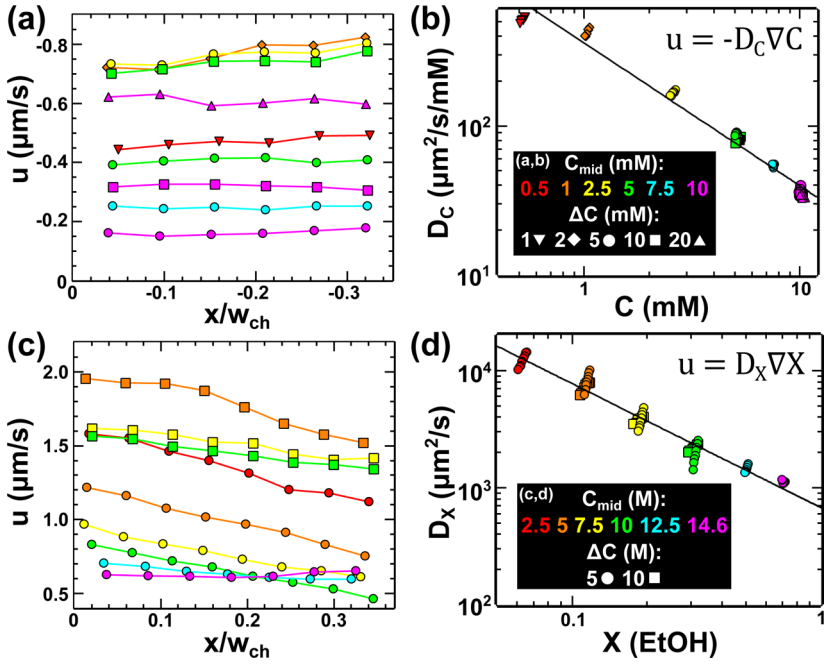

Figure 5. (a) Diffusiophoretic velocity measured at different positions within the analysis region (green box in Figure 4), with colors corresponding to midchannel concentrations c_{mid} ranging from 0.5 to 10 mM, and shapes corresponding to imposed concentration drops Δc ranging from 1 to 20 mM. A legend for the colors (c_{mid}) and shapes (Δc) appears in the inset to (b). (b) Diffusiophoretic mobility D_C (defined in eq 15) vs NaCl concentration. (c) Analogous solvophoretic velocity profiles in ethanol−water gradients, where the legend for the colors (c_{mid} ranging from 2.5 to 14.6 M) and shapes (Δc = 5 or 10 M) appears in the inset to (d). (d) Solvophoretic mobility D_X (eq 17) vs ethanol mole fraction X.

tration drop Δc results in a species flux j with a mass transfer resistance R_{tot} defined by

$$j = \frac{\Delta c}{R_{tot}} \tag{8}$$

Here R_{tot} is the sum of the channel R_{ch} and membrane R_m resistances

$$R_{tot} = 2R_m + R_{ch} \tag{9}$$

assuming that R_m is independent of concentration. The resistances are given by

$$R_{ch} = \frac{w_{ch}}{D} \tag{10}$$

$$R_m = \frac{w_m}{D_m} \tag{11}$$

with channel width w_{ch}, membrane width w_m, bulk diffusivity D, and membrane diffusivity D_m. Near the center of the membranes, the concentration profile can be assumed one-dimensional, and the steady profile is then

$$c(x) = \frac{c_L + c_R}{2} + \frac{R_{ch}}{R_{ch} + 2R_m}(c_R - c_L)\frac{x}{w_{ch}} \tag{12}$$

where c_L and c_R are the concentrations in the rapidly flowing left and right channel, respectively.

The effective membrane diffusivity for NaCl in PEG-DA membranes can be found in the literature (2.6×10^{-10} m^2/s, or D/D_m = 6.2, noting that this measurement was performed at 35 mM NaCl and using a slightly longer 13 monomer PEG chain,[35] but we assume it will serve as an adequate first approximation).

In ethanol−water solutions, the diffusivity in PEG-DA gels is not available in the literature. An estimate for this value is derived by assuming that both NaCl and ethanol diffusion obey the equation[36]

$$D_m = \frac{\varepsilon}{\tau}D \tag{13}$$

with void fraction ε and tortuosity τ. ε and τ are assumed to be independent of species such that D/D_m is assumed to be the same for ethanol and NaCl. Although the void volume may be slightly higher for the uncharged, smaller ethanol molecules, this assumption serves our purposes of calculating a first approximation of the mobility.

RESULTS AND DISCUSSION

Salt Diffusiophoresis: NaCl Gradients. Figure 5a shows the steady velocities measured for NaCl gradients. The middle channel concentration c_{mid} was varied between 0.5 and 10 mM, and concentration drop $\Delta c = c_R - c_L$ was varied between 1 and 20 mM. The measured velocities span a range of −0.2 to −0.8 μm/s and were directed toward higher NaCl concentration in the left channel. The velocity profiles were nearly uniform across the channel; at the lowest NaCl concentrations, the velocity varied by up to 0.1 μm/s across the channel. A general trend of higher velocity at lower concentration and higher gradient strength is clear.

We first investigate whether our measurements for NaCl diffusiophoresis show the expected concentration dependence. Diffusiophoretic velocities in electrolyte gradients are expected to obey eq 2, giving

$$u = D_{DP}\nabla \ln\left(\frac{c}{c^*}\right) = D_{DP}\frac{\nabla c}{c} \tag{14}$$

where D_{DP} is the diffusiophoretic mobility and includes both the electrophoretic and chemiphoretic contributions.[23] Our strategy will be to define a concentration-dependent mobility

$$D_C = -\frac{u}{\nabla c} \tag{15}$$

If the velocity measurements all collapse onto a single $D_C(c)$ curve, the velocity is indeed proportional to the gradient. For

DOI: 10.1021/acs.langmuir.5b00300
Langmuir XXXX, XXX, XXX−XXX

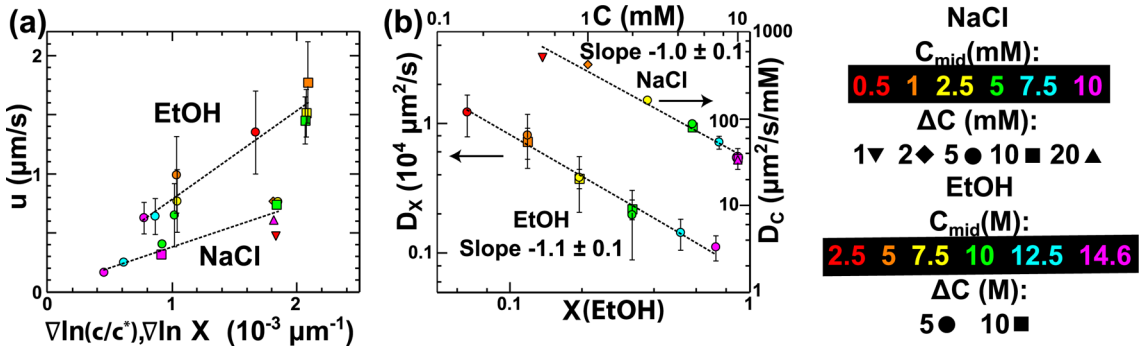

Figure 6. (a) Velocity of diffusiophoretic migration grows linearly with the logarithmic gradient of concentration or mole fraction, with slope equal to the diffusiophoretic mobility. (b) Diffusiophoretic mobilities D_C and D_X measured for NaCl and ethanol are inversely proportional to concentration (NaCl) and mole fraction (EtOH). Colors (c_{mid}) and shapes (Δc) are defined in the legend.

diffusiophoresis in salt gradients, $D_C \sim c^{-1}$ is expected from eq 14.

Figure 5b plots the diffusiophoretic mobility D_C against the concentration in the channel, calculated from eq 12. To confirm that diffusiophoretic velocities vary in proportion to the concentration gradient (eq 15), D_C was measured at c_{mid} = 5 and 10 mM multiple times by imposing various concentration drops Δc between 1 and 20 mM. Measured mobilities D_C exhibit a clear power-law dependence upon concentration, $D_C \sim c^{-0.96\pm0.04}$, such that

$$D_C = \frac{D_{DP}}{c} \tag{16}$$

verifies the logarithmic dependence of u in eq 14.

Solvophoresis: Ethanol Gradients. Next, the experimental system was used to measure solvophoretic velocities. The midpoint concentration c_{mid} of ethanol was varied between 2.5 and 14.6 M in water (5−70 mol % EtOH), and concentration drop Δc was set to either 5 or 10 M. Higher ethanol concentration was on the left and migration was observed to the right, toward lower ethanol concentration. Figure 5c shows the velocity profiles measured for each combination of c_{mid} and Δc. Measured velocities ranged from 0.5 to 2.0 μm/s, with velocity profiles that were somewhat nonuniform across the channel. Higher velocity was observed for larger gradients and lower ethanol concentration.

A clear relation was obtained when plotting the diffusiophoretic mobility against mole fraction X (rather than concentration)

$$D_X = \frac{u}{\nabla X} \tag{17}$$

Figure 5d shows the mobilities computed using eq 17. Mobilities measured with distinct concentration drops Δc = 5 and 10 M collapse onto a single curve, confirming that $U_{SP} \propto \nabla X$. Moreover, the solvophoretic mobility D_X exhibits a power-law dependence $D_X \sim X^{-1.06\pm0.06}$ on ethanol mole fraction. The solvophoretic velocity can therefore be described by

$$u = D_{SP} \nabla \ln X \tag{18}$$

where

$$D_{SP} = X D_X \tag{19}$$

One might understand the dependence of these phoretic mobilities D_{DP} (eq 14) and D_{SP} (eq 18) on $\nabla \ln(c/c^*)$ or $\nabla \ln X$, rather than ∇c and ∇X, in terms of the driving forces within the solution. Solution gradients naturally give rise to gradients in the chemical potentials of the solute or solvent molecules, which often have the form $\mu \sim k_B T \ln(c/c^*)$ or $\mu \sim k_B T \ln X$ in the ideal limit. Solute/solvent molecules in solution gradients thus experience thermodynamic driving forces $f \sim -\nabla\mu \sim -k_B T \nabla \ln(c/c^*)$ or $-k_B T \nabla \ln X$, which in turn drive the diffusio/solvophoretic migration. The EtOH/water mixtures in the present experiments are known to be nonideal, with partial molar volumes that change with composition. The consequences of these and other nonideal and multicomponent phenomena must be explored in developing a more fundamental understanding of solvophoresis.

Although eq 18 predicts the average velocity for a given experiment, the equation could not predict the individual velocity profiles. Measured mobilities slope in a direction opposite to the fit line, as was also observed at low ionic strengths for NaCl. This could be due to electrostatic interactions because of the small ionic strength of the ethanol−water solutions.

Figure 6b plots mobilities $\langle D_X \rangle$ and $\langle D_C \rangle$ averaged for each experiment against the concentrations X_{mid} and c_{mid} in the middle of the channel, with power-law fits that are consistent with those derived for D_X and D_C. The large error bars in $\langle D_X \rangle$ for ethanol arise primarily from the velocity spread in each experiment. Irrespective, a clear trend in D_X is evident.

Diffusio/solvophoretic mobilities D_{DP} and D_{SP} can be extracted from these measurements using eqs 14 and 18 and are shown in Table 1. Figure 6a shows the plots used to determine these mobilities. Moreover, the diffusiophoretic mobility may be related directly to the colloidal ζ-potential, via eqs 2 and 5, revealing a diffusiophoretically measured ζ-potential of $\zeta \sim -43 \pm 5$ mV, which is broadly consistent with the -59 ± 16 mV values measured electrophoretically using a Zetasizer Nano (Malvern Instruments).

Table 1. Mobilities from Diffusiophoresis and Solvophoresis Experiments

mobility	gradient	colloid	mobility ($\mu m^2/s$)
D_{DP}	NaCl−H_2O	1 μm PS	350 ± 60
D_{SP}	EtOH−H_2O	1 μm PS	760 ± 80

Diffusiophoresis in Diverse Chemical Gradients. While we have focused our quantitative measurements on diffusiophoresis in electrolyte gardients and solvophoresis in ethanol gradients, the technique presented in this paper can easily be adapted to a wide range of solute and solvent gradients. Figure 7 shows qualitative experiments in a variety of other solution

DOI: 10.1021/acs.langmuir.5b00300
Langmuir XXXX, XXX, XXX−XXX

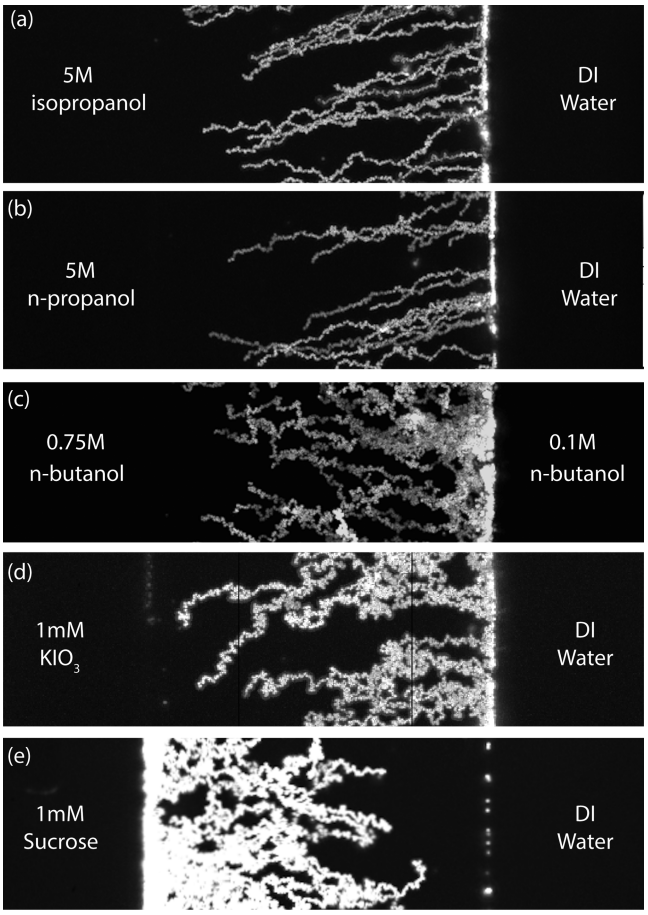

Figure 7. Streakline images of the solvo/diffusiophoretic migration of polystyrene colloids under various gradients: (a) isopropanol and (b) *n*-propanol, both of which are miscible with water; (c) *n*-butanol, which has a finite solubility in water; (d) the electrolyte KIO_3, in which PS particles migrate *down* the concentration gradient, unlike for most electrolytes; and (e) sucrose, a nonelectrolyte solute.

gradients. PS particles migrate *down* gradients in solutions of the water-miscible alcohols isopropanol (Figure 7a, with c_{mid} = 2.5 M and Δc = 5 M) and *n*-propanol (7b, with c_{mid} = 2.5 M and Δc = 5 M), just like in ethanol gradients. Gradients of solvents with finite solubility can also be imposed, with Figure 7c showing diffusiophoresis down *n*-butanol gradients (with c_{mid} = 425 mM and Δc = 650 mM). Figure 7d shows PS colloids to migrate *down* gradients in the electrolyte KIO_3 (c_{mid} = 0.5 mM and Δc = 1 mM), which is opposite the direction in the vast majority of electrolytes. In this case, the diffusivity of the K^+ anion is higher than that of the IO_3^- anion, so that the electro-diffusiophoretic and chemi-diffusiophoretic components of eq 2 are oppositely directed. Moreover, the electro-diffusiophoretic component exceeds the chemi-diffusiophoretic component[29] and therefore drives colloids down the ionic strength gradient. Finally, Figure 7e shows diffusiophoretic migration in a nonelectrolyte gradient (sucrose, c_{mid} = 0.5 mM and Δc = 1 mM), wherein PS colloids migrate *up* the sucrose gradient.

DISCUSSION AND CONCLUSION

The experimental system described here enables the direct visualization of diffusiophoretic migration under diverse chemical gradients. This was applied to measure the velocity under NaCl and ethanol concentration gradients and compute the resulting mobility. The diffusiophoretic velocity in NaCl gradients showed a $u \sim \nabla \ln(c/c^*)$ dependence, as expected from theory and literature. The solvophoretic velocity was found to obey a $u \sim \nabla \ln X$ dependence.

Although we have assumed that the colloidal migration visualized here reflects diffusiophoresis alone, diffusioosmotic flows (DOF) might also be driven within the channel by solution gradients, whether established along channel walls or within the hydrogel membranes. Such DOF would contribute to the migration velocity measured for the beads and would be (erroneously) interpreted as contributing to diffusiophoresis. Despite this possibility, we do not believe DOF contributes significantly in our experiments. Unless the total diffusioosmotic flux through the membrane were identical to that along the walls, a pressure-driven backflow would necessarily arise to ensure mass conservation. Such pressure-driven backflows would introduce a (parabolic) component to the velocity profile across the depth of the channel (as would occur with electroosmosis, as shown in Supplemental Video 5 in ref 27). Particle motion, however, is measured to be very nearly uniform across the channel height, suggesting that diffusioosmosis does not contribute significantly to our measured mobilities.

Osmotic pressure differences may also exist between the two solutions separated by the hydrogel membrane, which could drive an osmotic flow through the gel. As a first approximation, the osmotic pressure of a solution scales inversely with the molar volume of the solution, which here often implies that osmotic pressures are larger for larger water mole fractions. In the paradigmatic case of a semipermeable membrane, osmotic pressure differences drive water to flow toward the less dilute solution. The situation is more complicated in the solvophoresis experiments presented here, since the hydrogel membrane is permeable to both species in the binary solutions on either side. Nonetheless, we would expect osmotic pressure differences to drive water (and thus flow) toward lower water concentrations, which would in turn advect colloids toward lower water concentrations. By contrast, we generally observe colloids to move *down* solvent gradients. Finally, any putative osmotic pressure-driven flow would introduce a parabolic contribution to the colloidal velocity profile—as would occur for DOF—which is absent in our measurements.

Many measurements described here used deionized water in one reservoir channel to act as a "sink" for the solute/solvent introduced in the other. Water absorbs atmospheric carbon dioxide, forming a weak carbonic acid solution. Typical DI water has pH 5.5−6 and typically contains 1−5 μM of carbonate ions, which are not treated in our analysis.[37] Our results would thus be suspect anywhere that this (unknown) carbonate concentration comprised an appreciable fraction of the solute in solution. This is never the case in any experiments reported here: the hydrogel membranes are thick enough that the concentration everywhere within the sample channel is of order c_{mid}, which is of order 10^3 higher than the carbonate concentration. We opted against buffering the solutions described here, as this would require ∼10 mM buffer concentrations that would overwhelm most of the gradients we sought to impose. Similarly, we used water to act as a sink for the solvent to avoid multicomponent coupling of solvent and buffer (or electrolyte) fluxes in our solvophoresis experiments.

DOI: 10.1021/acs.langmuir.5b00300
Langmuir XXXX, XXX, XXX−XXX

The experimental system shown here can measure diffusiophoretic mobilities for a wide variety of particles, in a wide variety of solutions. We envision this technique will provide a versatile new tool for the characterization and manipulation of colloids, much like electrophoretic mobility measurements are now routinely used to measure ζ-potentials for colloids of different sizes or surface chemistries in solutions of different composition. Such direct measurements should enable mechanisms for solvophoresis to be hypothesized and tested, as has recently occurred with experimental and theoretical studies in thermophoresis.[38,39] Kosmulski and Matuevi originally hypothesized that hydration gradients along the colloid surface drive solvophoretic migration,[26] but other forces could also arise in multicomponent mixtures. We have identified various mechanisms that could be responsible for the solvophoretic migration observed here. Solvent/surface interaction forces (e.g., hydration/solvation or van der Waals) could give rise to an adsorption layer, as computed in eq 1. In any multicomponent mixture, gradients of one species may drive the flux of another; e.g., solvent gradients may drive electrolyte fluxes (and therefore diffusiophoresis in the electrolyte gradient). Surface charge density may depend on local solvent composition (e.g., surface acid groups may reprotonate with increasing EtOH fraction). Because electrical permittivity depends on solvent composition, solvent gradients establish nonuniform screening lengths λ_D along the particle surface, which would also drive migration.

A more general understanding of such mechanisms—both theoretical and experimental—will be required for the conceptual design and engineering of particles that migrate solvophoretically in a prescribed fashion. The manipulation and migration of such engineered particles could benefit a number of subsurface energy harvesting and environmental applications. For example, naturally occurring or induced chemical gradients can be utilized to drive the phoretic migration of naturally occurring or engineered nanoparticles to target regions for beneficial alterations or to autonomously seek out regions rich in particular components.

This experimental work has unveiled the functional dependence of the solvophoretic velocity on concentration and gradient strength, which was enabled by the improved accuracy granted by direct visualization. The groundwork has been laid for future studies using salt, surfactant, polymers, and various colloidal systems to develop an enhanced understanding of solvophoresis as well as other types of diffusiophoresis using novel chemistries.

AUTHOR INFORMATION

Corresponding Author

*E-mail: squires@engineering.ucsb.edu (T.M.S.).

Notes

The authors declare no competing financial interest.

ACKNOWLEDGMENTS

We gratefully acknowledge support from the Institute for Collaborative Biotechnologies through Grant W911NF-09-0001 from the U.S. Army Research Office, from Saudi Aramco under ASC Contract 600013692, the ACS Petrolem Research Foundation under Grant 54141-ND5, and the NSF under Grant CBET-1438779. The content of the information does not necessarily reflect the position or the policy of the U.S. Government or Saudi Aramco, and no official endorsement should be inferred. A portion of this work was performed in the UCSB Nanofabrication Facility, part of the NSF-funded NNIN network, and in the Materials Research Laboratory Central Facilities, which are supported by the NSF Materials Research Science and Engineering Centers Program under Grant DMR 1121053, a member of the NSF-funded Materials Research Facilities Network.

REFERENCES

(1) Deryaguin, B. V.; Dukhin, S. S.; Korotkova, A. A. Diffusiophoresis in electrolyte solutions and its role in the mechanism of film formation from rubber latexes by the method of ionic deposition. *Kolloidn. Zh.* **1961**, *23*, 53.

(2) Lin, M. M. J.; Prieve, D. C. Electromigration of latex induced by a salt gradient. *J. Colloid Interface Sci.* **1983**, *95*, 327−339.

(3) Ebel, J. P.; Anderson, J. L.; Prieve, D. C. Diffusiophoresis of latex particles in electrolyte gradients. *Langmuir* **1988**, *4*, 396−406.

(4) Anderson, J. L. Colloid Transport by Interfacial Forces. *Annu. Rev. Fluid Mech.* **1989**, *21*, 61−99.

(5) Deryaguin, B. V.; Sidorenkov, G.; Zubashchenko, E.; Kiseleva, E. Kinetic Phenomena in the Boundary Layers of Liquids 1. The Capillary Osmosis. *Kolloidn. Zh.* **1947**, *9*, 335−347.

(6) Smith, R. E.; Prieve, D. C. Accelerated deposition of latex particles onto a rapidly dissolving steel surface. *Chem. Eng. Sci.* **1982**, *37*, 1213−1223.

(7) Kar, A.; Guha, R.; Dani, N.; Velegol, D.; Kumar, M. Particle deposition on microporous membranes can be enhanced or reduced by salt gradients. *Langmuir* **2014**, *30*, 793−799.

(8) Paxton, W. F.; Kistler, K. C.; Olmeda, C. C.; Sen, A., St.; Angelo, S. K.; Cao, Y.; Mallouk, T. E.; Lammert, P. E.; Crespi, V. H. Catalytic nanomotors: Autonomous movement of striped nanorods. *J. Am. Chem. Soc.* **2004**, *126*, 13424−13431.

(9) Moran, J. L.; Posner, J. D. Electrokinetic locomotion due to reaction-induced charge auto-electrophoresis. *J. Fluid Mech.* **2011**, *680*, 31−66.

(10) Brady, J. F. Particle motion driven by solute gradients with application to autonomous motion: continuum and colloidal perspectives. *J. Fluid Mech.* **2011**, *667*, 216−259.

(11) Golestanian, R.; Liverpool, T.; Ajdari, A. Propulsion of a molecular machine by asymmetric distribution of reaction products. *Phys. Rev. Lett.* **2005**, *94*, 220801.

(12) Ibele, M.; Mallouk, T. E.; Sen, A. Schooling behavior of light-powered autonomous micromotors in water. *Angew. Chem., Int. Ed.* **2009**, *48*, 3308−3312.

(13) Theurkauff, I.; Cottin-Bizonne, C.; Palacci, J.; Ybert, C.; Bocquet, L. Dynamic clustering in active colloidal suspensions with chemical signaling. *Phys. Rev. Lett.* **2012**, *108*, 268303.

(14) Buttinoni, I.; Volpe, G.; Kümmel, F.; Volpe, G.; Bechinger, C. Active Brownian motion tunable by light. *J. Phys.: Condens. Matter* **2012**, *24*, 284129.

(15) Florea, D.; Musa, S.; Huyghe, J. M. R.; Wyss, H. M. Long-range repulsion of colloids driven by ion exchange and diffusiophoresis. *Proc. Natl. Acad. Sci. U. S. A.* **2014**, *111*, 6554−6559.

(16) McDermott, J. J.; Kar, A.; Daher, M.; Klara, S.; Wang, G.; Sen, A.; Velegol, D. Self-generated diffusioosmotic flows from calcium carbonate micropumps. *Langmuir* **2012**, *28*, 15491−15497.

(17) Prieve, D. C. Migration of a colloidal particle in a gradient of electrolyte concentration. *Adv. Colloid Interface Sci.* **1982**, *16*, 321−335.

(18) Staffeld, P. O.; Quinn, J. A. Diffusion-induced banding of colloid particles via diffusiophoresis: 2. Non-electrolytes. *J. Colloid Interface Sci.* **1989**, *130*, 88100.

(19) Squires, T. M.; Quake, S. R. Microfluidics: Fluid physics at the nanoliter scale. *Rev. Mod. Phys.* **2005**, 977.

(20) Abécassis, B.; Cottin-Bizonne, C.; Ybert, C.; Ajdari, A.; Bocquet, L. Boosting migration of large particles by solute contrasts. *Nat. Mater.* **2008**, *7*, 785−789.

DOI: 10.1021/acs.langmuir.5b00300
Langmuir XXXX, XXX, XXX−XXX

(21) Abécassis, B.; Cottin-Bizonne, C.; Ybert, C.; Ajdari, A.; Bocquet, L. Osmotic manipulation of particles for microfluidic applications. *New J. Phys.* **2009**, *11*, 075022.
(22) Palacci, J.; Abécassis, B.; Cottin-Bizonne, C.; Ybert, C.; Bocquet, L. Colloidal motility and pattern formation under rectified diffusiophoresis. *Phys. Rev. Lett.* **2010**, *104*, 138302.
(23) Palacci, J.; Cottin-Bizonne, C.; Ybert, C.; Bocquet, L. Osmotic traps for colloids and macromolecules based on logarithmic sensing in salt taxis. *Soft Matter* **2012**, *8*, 980.
(24) Anderson, J. L.; Lowell, M. E.; Prieve, D. C. Motion of a particle generated by chemical gradients. Part 1. Non-electrolytes. *J. Fluid Mech.* **1982**, *117*, 107−121.
(25) Khair, A. S. Diffusiophoresis of colloidal particles in neutral solute gradients at finite Peclet number. *J. Fluid Mech.* **2013**, *731*, 64−94.
(26) Kosmulski, M.; Matuevi, E. Solvophoresis of latex. *J. Colloid Interface Sci.* **1992**, *150*, 291−294.
(27) Paustian, J. S.; Azevedo, R. N.; Lundin, S.-T. B.; Gilkey, M. J.; Squires, T. M. Microfluidic microdialysis: Spatiotemporal control over solution microenvironments using integrated hydrogel membrane microwindows. *Phys. Rev. X* **2013**, *3*, 041010.
(28) Bartolo, D.; Degré, G.; Nghe, P.; Studer, V. Microfluidic stickers. *Lab Chip* **2008**, *8*, 274−279.
(29) Prieve, D. C.; Anderson, J. L.; Ebel, J. P.; Lowell, M. E. Motion of a particle generated by chemical gradients. Part 2. Electrolytes. *J. Fluid Mech.* **1984**, *148*, 247−269.
(30) Chiang, T.-Y.; Velegol, D. Multi-ion diffusiophoresis. *J. Colloid Interface Sci.* **2014**, *424*, 120−123.
(31) Bruus, H. *Theoretical Microfluidics*; Oxford University Press: Oxford, UK, 2008; Vol. *18*.
(32) Mansuripur, T. S.; Pascall, A. J.; Squires, T. M. Asymmetric flows over symmetric surfaces: capacitive coupling in induced-charge electro-osmosis. *New J. Phys.* **2009**, *11*, 075030.
(33) Werely, S. T.; Meinhart, C. D. Recent advances in micro-particle image velocimetry. *Annu. Rev. Fluid Mech.* **2010**, *42*, 557−576.
(34) Raffel, M. *Particle Image Velocimetry: A Practical Guide*; Springer: Berlin, 2007.
(35) Sagle, A. C.; van Wagner, E. M.; Ju, H.; McCloskey, B. D.; Freeman, B. D.; Sharma, M. M. PEG-coated reverse osmosis membranes: Desalination properties and fouling resistance. *J. Membr. Sci.* **2009**, *340*, 92−108.
(36) Cussler, E. L. *Diffusion: Mass Transfer in Fluid Systems*; Cambridge University Press: New York, 2009.
(37) Persat, A.; Suss, M. E.; Santiago, J. G. *Lab Chip* **2009**, *9*, 2454−2469.
(38) Duhr, S.; Braun, D. Why molecules move along a temperature gradient. *Proc. Natl. Acad. Sci. U. S. A.* **2006**, *103*, 19678−19682.
(39) Würger, A. Thermal non-equilibrium transport in colloids. *Rep. Prog. Phys.* **2010**, *73*, 126601.

DOI: 10.1021/acs.langmuir.5b00300
Langmuir XXXX, XXX, XXX−XXX